Positronium emission from mesoporous silica studied by laser-enhanced time-of-flight spectroscopy

2015 New J. Phys. 17 043059

(http://iopscience.iop.org/1367-2630/17/4/043059)

New Journal of Physics
The open access journal at the forefront of physics

Deutsche Physikalische Gesellschaft DPG
IOP Institute of Physics

Published in partnership with: Deutsche Physikalische Gesellschaft and the Institute of Physics

OPEN ACCESS

RECEIVED
9 December 2014

REVISED
11 March 2015

ACCEPTED FOR PUBLICATION
24 March 2015

PUBLISHED
28 April 2015

PAPER

Positronium emission from mesoporous silica studied by laser-enhanced time-of-flight spectroscopy

A Deller, B S Cooper, T E Wall and D B Cassidy

Department of Physics and Astronomy, University College London, Gower Street, London, WC1E 6BT, UK

E-mail: a.deller@ucl.ac.uk **and** d.cassidy@ucl.ac.uk

Keywords: antimatter, positronium, diffusion, tunnelling, mesoporous silica

Abstract

The use of mesoporous silica films for the production and study of positronium (Ps) atoms has become increasingly important in recent years, providing a robust source of free Ps in vacuum that may be used for a wide variety of experiments, including precision spectroscopy and the production of antihydrogen. The ability of mesoporous materials to cool and confine Ps has also been utilized to conduct measurements of Ps–Ps scattering and Ps_2 molecule formation, and this approach offers the possibility of making a sufficiently dense and cold Ps ensemble to realize a Ps Bose–Einstein condensate. As a result there is great interest in studying the dynamics of Ps atoms inside such mesoporous structures, and how their morphology affects Ps cooling, diffusion and emission into vacuum. It is now well established that Ps atoms are initially created in the bulk of such materials and are subsequently ejected into the internal voids with energies of the order of 1 eV, whereupon they rapidly cool via hundreds of thousands of wall collisions. This process can lead to thermalisation to the ambient sample temperature, but will be arrested when the Ps deBroglie wavelength approaches the size of the confining mesopores. At this point diffusion through the pore network can only proceed via tunneling, at a much slower rate. An important question then becomes, how long does it take for the Ps atoms to cool and escape into vacuum? In a direct measurement of this process, conducted using laser-enhanced positronium time-of-flight spectroscopy, we show that cooling to the quantum confinement regime in a film with approximately 5 nm diameter pores is nearly complete within 5 ns, and that emission into vacuum takes ∼10 ns when the incident positron beam energy is 5 keV. The observed dependence of the Ps emission time on the positron implantation energy supports the idea that quantum confined Ps does not sample all of the available pore volume, but rather is limited to a subset of the mesoporous network.

1. Introduction

Positronium (Ps) is a metastable hydrogenic atomic system composed of a positron bound to an electron [1] and has numerous applications in both fundamental [2] and applied [3] physics and chemistry. Positrons implanted into solid materials [4] may produce positronium via several distinct mechanisms [5–11], and with a wide range of properties. Measurements of these properties can provide useful information about Ps forming materials; for example, the kinetic energy of Ps emitted from metal surfaces can be used to deduce the electronic density of states thereupon [12, 13].

Recently there have been significant developments in the use of Ps as a probe of mesoporous materials, which are of use in the semiconductor industry as low-κ interlayer dielectrics [10]. When positrons are implanted into these materials Ps atoms may be generated in the internal voids (typically with positron-positronium conversion efficiencies in the range of 20–50%). Measurements of subsequent Ps lifetimes can be used to determine important material parameters, such as porosity and tortuosity, even when the pores are not accessible to the vacuum [14, 15].

The same characteristics that make Ps an efficient probe of mesoporous materials can be exploited to create useful sources of Ps. By creating Ps atoms inside a porous structure many interesting experiments become possible. For example, cold Ps emitted from a silica film was instrumental in the resolution of a long-standing discrepancy between calculations and measurements of the ortho-Ps lifetime [16], and confined Ps was probed optically to study cavity shifts and line narrowing [17]. Moreover, the voids in mesoporous targets keep Ps atoms quasi-localized, which facilitated the first observation of Ps–Ps interactions [18] and the subsequent discovery of molecular positronium (Ps_2) [19].

Mesoporous materials with interconnected pore structures [20] provide a natural cooling mechanism, since confined Ps atoms may interact strongly with the pore surfaces without being destroyed [14]. Indeed, it has been shown in several studies ([21, 22]) that Ps will rapidly cool down to the lowest energy levels allowed by the confining volumes [23]. When this happens, and the Ps deBroglie wavelength is comparable to the confining pore size, the Ps is said to be quantum confined, although it may still escape into vacuum if the pore structure allows. Ps that has not reached the quantum confinement regime will be emitted from the samples very quickly, whereas quantum confined Ps will take significantly longer. Hot Ps will sample all pores equally in a normal random walk process, having, in effect, a time-dependent diffusion coefficient, but quantum confined Ps will tunnel from pore to pore with a nearly constant diffusion coefficient [24]. Both of these scenarios are difficult to model and require detailed knowledge of the pore structure that is usually not available. We note that our discussion here refers only to silica films, but many other materials can be used to create mesoporous structures (e.g., [25]) and in general our arguments would apply to those as well.

Because quantum confinement can set a lower limit on the minimum energy with which Ps atoms can be emitted into vacuum, it is not always possible to correlate the free Ps kinetic energy with other parameters (e.g., implantation depth) to obtain information about the Ps dynamics in a porous network [26]. We show here that time-of-flight (TOF) measurements can reveal Ps cooling and emission times directly, without any model-dependent assumptions concerning Ps dynamics prior to emission. We report measurements of the longitudinal Ps velocity, v_z, made using the technique of laser-enhanced positronium time-of flight (LEPTOF) spectroscopy. This is a technique wherein the pulsed output from a buffer gas positron trap [27] generates Ps atoms which are subsequently photoionized with pulsed lasers at a well defined time and location. Detection of the annihilation of liberated positrons makes it possible to construct a TOF spectrum utilizing a large fraction of the available Ps atoms, in contrast to conventional Ps TOF measurements which rely on the spontaneous decay of Ps atoms that happen to be in the field of view of the detector [28]. By performing such measurements at different positron beam energies, and with the laser at different distances from the target, we obtain the mean time for Ps emission and for cooling to the quantum confinement regime.

2. Methods

2.1. Positron beamline and positronium production

The positron beam and trap system is very similar to that described in [29], the main difference being that the output from the two-stage trap was used directly (i.e., there is no pulse stacking in a secondary high-vacuum accumulator). The trap was operated at 1 Hz, delivering over 10^5 positrons per pulse with a time-width of ~ 5 ns (FWHM). Time-bunching was achieved by applying fast voltage pulses (120–170 V) to the trapping electrodes, creating an approximately linear potential [30]. The magnetic field generated by the trap solenoid is ~600 G, compared to ~100 G in the target region, resulting in a beam spot size on the SiO_2 film of around 5 mm.

The silica target used in this work was grown using Pluronic F-127 ethyleneoxide/propyleneoxide block copolymer (BASF) with a 0.016 F-127/Si molar ratio, spin coated onto a silicon substrate [31]. The 360 mm^2 silica film is approximately 1 μm in thickness with pores estimated to be $d \sim 5$ nm in diameter. Similar films have been shown to emit Ps to vacuum with high efficiency (~30%) and at low emission energies ($E_{Ps} < 0.1$ eV) [22, 32]. The positron beam was implanted into the film with between 500 eV and 5 keV, resulting in a range of different positronium velocity distributions.

2.2. Positron annihilation lifetime spectroscopy

Annihilation γ-radiation was measured with a lead tungstate ($PbWO_4$) scintillator crystal [33] optically coupled to a photomultiplier tube (PMT). A 50 Ω splitter was used to divide the PMT signal between two channels of a 1 GHz, 12 bit digital oscilloscope (Teledyne Lecroy, HDO 4104). The waveforms from each channel were then spliced together and a constant fraction discriminator (CFD) algorithm employed to determine the trigger time ($t = 0$), configured for the leading-edge of the prompt peak (see figure 1). This technique is known as single-shot positron annihilation lifetime spectroscopy (SSPALS) [34].

Single-shot lifetime spectra can be analyzed in a number of different ways. One convenient metric is the integral of the delayed annihilation events, normalized against the entire signal:

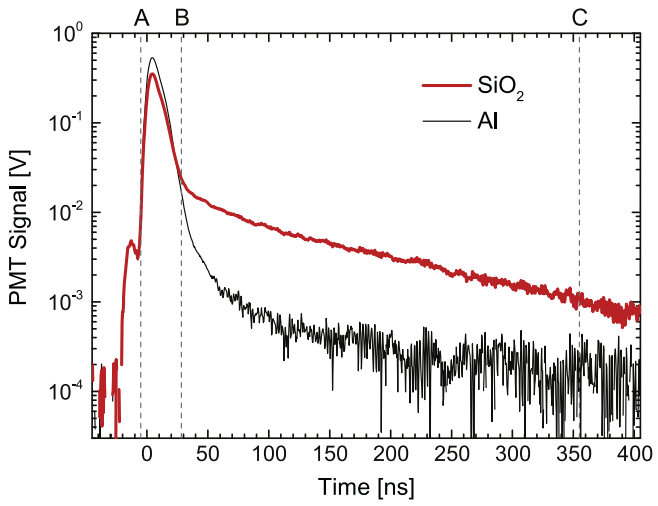

Figure 1. Lifetime spectra for 1 keV positrons implanted into an aluminium (black) or porous silica (red) target. The untreated Al surface is not expected to produce a significant amount of Ps, whereas the delayed signal evident from the silica target indicates positron to o-Ps conversion efficiency of ≈25%. The step at around $t = -10$ ns is due to positrons annihilating on a pumping restriction aperture downstream from the target region.

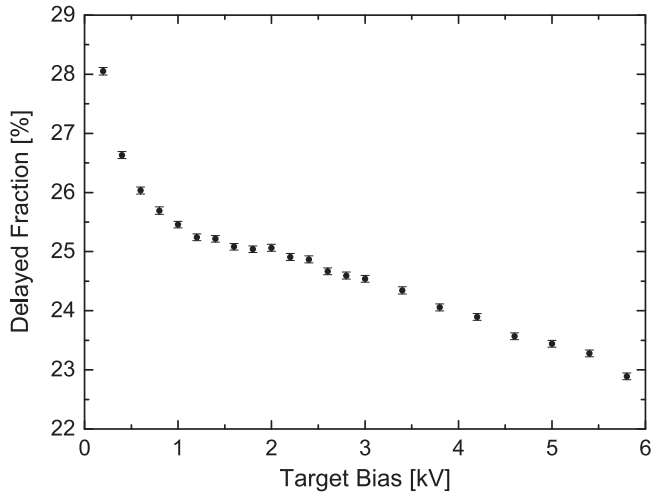

Figure 2. The SSPALS measured delayed fraction for positrons implanted into F-127 mesoporous silica with the target biased from 200 V to 5.8 kV. The sharp increase in f below 1 kV is attributed to positrons reflected from the surface. The background (no Ps) fraction of around 3% has not been subtracted.

$$f = \int_B^C V(t)\ \mathrm{d}t \Big/ \int_A^C V(t)\ \mathrm{d}t. \tag{1}$$

Here $V(t)$ is the PMT output voltage (see figure 1). The delayed fraction f gives an indication of the amount of long-lived Ps formed [26]. Typically we assign $A = -3$ ns, $B = 35$ ns, and $C = 350$ ns. Figure 2 shows how measurements of f vary for positrons implanted to different depths inside porous silica, demonstrating that for those implanted deepest fewer Ps atoms are subsequently emitted. These data were recorded with the detector sufficiently far away from the Ps source to preclude any significant effect on its solid angle coverage due to the (energy-dependent) flight path. The 2% reduction in the Ps signal (bias >2 kV) per keV implantation energy K is consistent with previous observations using nominally identical samples [22].

We note that this method of analysis is only useful for events that occur shortly after the Ps is produced (i.e., in the time window AB, figure 1). For events at arbitrary times beyond this window other analysis methods must be used, as described in section 2.4.

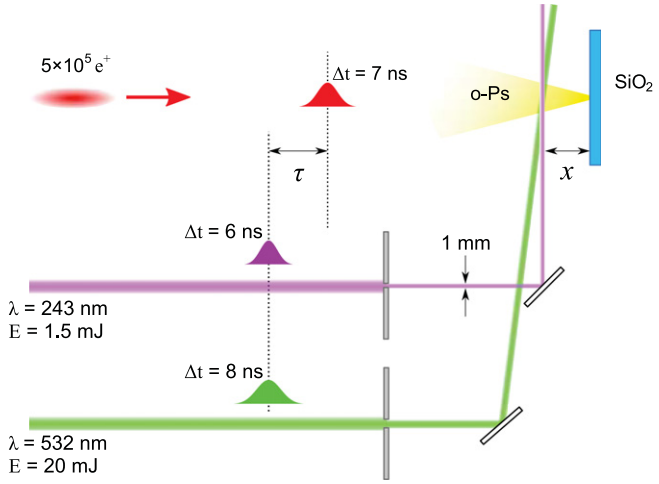

Figure 3. Schematic illustration of the LEPTOF arrangement. Positrons (red) from the two-stage trap are implanted into a porous silica target (blue) that re-emits positronium atoms (yellow). These may then be photoionized by the 243 nm (purple) and 532 nm (green) pulsed lasers. The Ps TOF is mapped using the ionization signal, as both the time between releasing the positrons and triggering the laser Q-switch (τ) and the distance between the lasers and target (z), are each varied.

2.3. Lasers

The 1s–2p transition of Ps can be driven by a single photon of wavelength $\lambda = 243$ nm. To produce such light we used the second harmonic of a pulsed dye laser (Sirah Cobra-P, operated with coumarin 102 dye), pumped by the third harmonic of a pulsed Nd:YAG laser (Surelite II-10, with up to 160 mJ/pulse at 355 nm). Three SF10 glass prisms make up the dispersive element inside the resonator of the dye laser, which generates radiation with a relatively large bandwidth of $\Delta\nu = 60$ GHz at $\lambda = 486$ nm. A BBO crystal frequency-doubles the output to $\lambda = 243$ nm in a 6 ns (FWHM) pulse, with a maximum energy of 5 mJ and a bandwidth of $\Delta\nu \approx 85$ GHz. The doubling efficiency was controlled by varying the phase-matching angle of the crystal, enabling regulation of the output UV energy as the laser wavelength was scanned over the 1s–2p transition. The UV beam was expanded with a telescope then passed through a thin slit. The UV intensity profile was measured to be near Gaussian along the horizontal axis (FWHM $\sim$ 0.6 mm), with a uniform 'top-hat' distribution (6 mm across) in the vertical direction.

The excited ($n = 2$) Ps atoms were photoionized using the residual second harmonic radiation from the Nd:YAG (visible, $\lambda = 532$ nm), which enters the vacuum chamber through the same window as the UV radiation. Approximately 20 mJ in a 7 ns (FWHM) pulse was used for photoionization. The two lasers were made to overlap in the centre of the chamber, in front of the Ps converter. The path of the 532 nm beam includes a 1.5 m long delay, designed such that both the visible and UV radiation arrive simultaneously at the overlap region.

The Q-switch of the Nd:YAG was operated at a repetition rate of 1 Hz, matching the loading time of the positron trap, whereas the flash-lamps were triggered at 10 Hz, to maintain thermal equilibrium inside the laser rod.

2.4. Experimental procedure

The velocity of the Ps atoms emitted into vacuum from the mesoporous silica converter [32] was determined using LEPTOF spectroscopy. This technique employs a spatially well-defined probe laser (see section 2.3), aligned parallel to the target, which is fired at time τ relative to the arrival of positrons, and that intersects the resulting Ps at a distance z from the target surface, as shown in figure 3.

In this work, two overlapping lasers ($\lambda = 243$ nm and $\lambda = 532$ nm) were employed to probe the Ps atoms via resonance-enhanced multi-photon ionization (REMPI) [35]. Although both lasers are required for photoionization, it is the profile of the UV beam that predominately determines the spatial resolution of the LEPTOF measurement. In figure 4 we show calculations for the ionization probability as a function of Ps velocity through the laser fields (assuming no Doppler shift). For experiments conducted in higher magnetic fields one could dispense with the ionization laser entirely and use the magnetic quenching signal arising from the mixing of 2p singlet and triplet states [36].

Photoionized positrons are accelerated back to the target by the same electric field that defines the incident beam energy. The time between photoionization and positron impact varies depending on where in the field the former occurs, but even the slowest positrons will reach the target in less than 1 ns. The majority (~70%) of these positrons will promptly annihilate and generate an excess of γ-ray photons in the lifetime spectra during a time

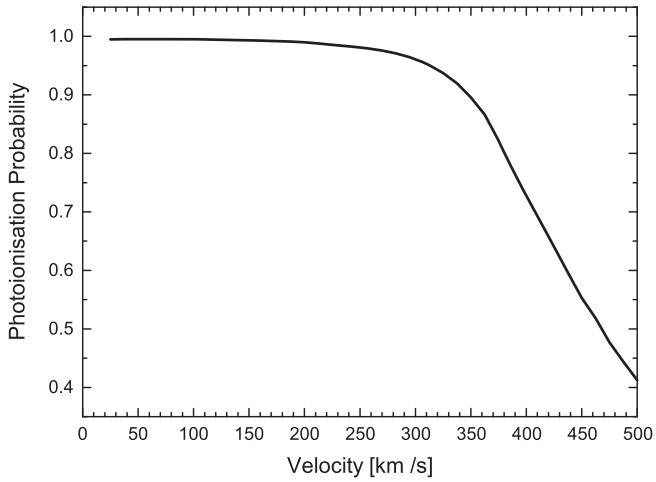

Figure 4. Calculated photoionization probability of Ps travelling through the laser interaction region. The laser pulses are as described in section 2.3. See appendix for details of the calculation.

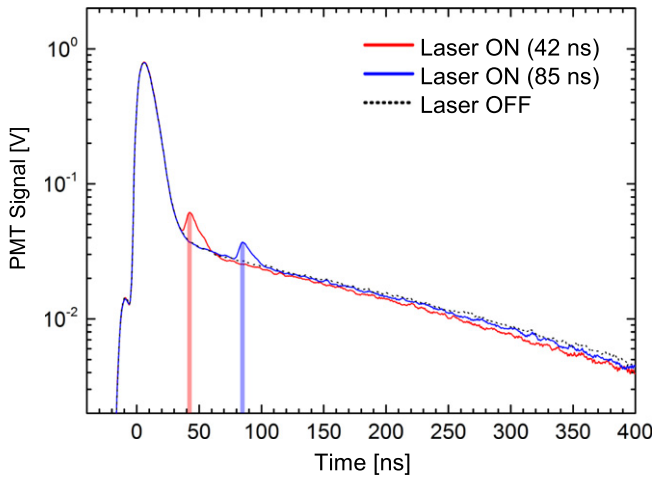

Figure 5. SSPALS spectra recorded with the laser centred 3.25 mm from the target and the UV beam tuned on/ off resonant (243.02 nm / 242.25 nm) for different delays, indicated by the 4 ns shaded regions.

window correlated with the laser pulse. This signal is related to the fraction of atoms within the profile of the UV laser during the 6 ns pulse.

Figure 5 shows three example lifetime spectra that have been normalized by the signal integrated from −3 to 350 ns, and averaged over approximately 120 shots. In two cases (red, blue) the lasers were applied with the UV beam tuned to the 1s–2p interval ($\lambda = 243$ nm) and delayed relative to the positron trigger by 42 and 85 ns, respectively. The shaded regions indicate a 4 ns window centred about the arrival of the laser. An excess is evident, coincident with the laser, in comparison to the background measurement (black) for which the UV laser was detuned from resonance to $\lambda = 242.25$ nm. For these measurements the target was biased to 5 kV and the lasers centred 3.25 mm from its surface.

Series of lifetime spectra were recorded for a wide range of laser delays ($\tau = -10$ to 190 ns), and with the UV wavelength alternated between on and off resonance. For each delay we then measured the difference in signal between the two wavelength tunings and determined the fraction of the Ps atoms which had been resonantly ionized by the lasers, assuming these naturally decay with a mean lifetime of 142 ns. Figure 6 shows a range of background subtracted and decay corrected spectra $[V_{\mathrm{on}}(t) - V_{\mathrm{off}}(t)] \cdot \mathrm{e}^{t/142\ \mathrm{ns}}$, demonstrating an excess that correlates with the timing of the laser. To quantify the excess signal we used a 4 ns interval of each background-subtracted spectrum, centred at the laser arrival time (e.g. the time windows shaded in figures 5 and 6), and calculate the mean value (W) within this region. Unlike the delayed fraction f, the parameter W allows us to observe changes in the annihilation radiation signal at times long after the prompt annihilation peak.

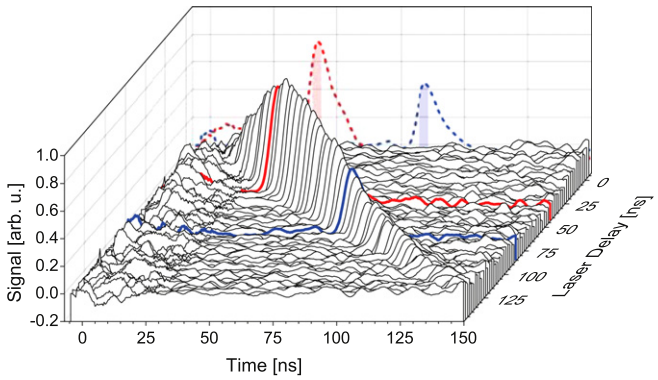

Figure 6. Background-subtracted, normalized and o-Ps decay corrected SSPALS spectra for various laser delay times ($\tau = 42$ ns / 85 ns highlighted red/ blue and projected on to the rear panel—dashed); the delay interval is 2.5 ns. The diagonal ridge indicates an excess in annihilations due to REMPI of the Ps atoms passing through the beam. The shaded regions indicate the 4 ns measurement windows.

Furthermore, we can also observe effects that overlap with the prompt peak (with reduced statistics), in contrast to conventional Ps TOF methods.

The total emission and flight time was defined to be the interval between the main peak in the SSPALS spectra (positron implantation) and the arrival of the laser. The latter was determined using the absolute trigger time of the laser Q-switch, adjusted using the offset found by measuring the timing of the prominent background-subtracted peaks.

3. Results and discussion

3.1. TOF distributions

The LEPTOF technique gives the arrival time of Ps atoms at a particular point in space, relative to the mean implantation time of the positrons. This is a convolution of the time-width of the incident positron bunch and the Ps velocity distribution, as well as the range of emission times for Ps from the sample. In figure 7 we plot the excess gamma-ray ionization signal W, against laser delay for various values of the target bias and flight path z. Following [37], an asymmetrical double sigmoid function was fitted to the spectra. This function is not based on a physical model for the distribution but was found to fit the data well.

As slower atoms take longer to traverse the interaction region and can therefore be photoionized within a broader time window than faster atoms, they will effectively be over-counted in the spectra to a degree inversely proportional to their speed. To account for this a correction function of t^{-1} was applied to the TOF spectra fits. The distributions were truncated to a minimum time equivalent to a velocity of 440 km s^{-1} (i.e. a kinetic energy of 1.1 eV—the maximum expected [22]), for each measurement distance. Furthermore, the photoionization probability will vary as a function of the speed of a given Ps atom, and for very high speeds the transit time is too short to have any chance of producing a detectable signal. We calculate that for our combination of lasers the probability is close to one (on resonance) for $v_z \lesssim 300$ km s^{-1}, above which the likelihood is steadily reduced. The TOF spectra fits were then corrected for this effect by dividing by the calculated photoionization probability function (figure 4).

The mean time for Ps to reach each measurement region was then determined using the expectation value $\langle t \rangle$ of each corrected fit. By extrapolation it was possible to suitably normalize the function, even for those data-sets that are cut off at long times (i.e., for the longest flight paths). Figure 8 shows the mean flight plus emission time to the point where, on average, photoionization took place (relative to the target surface): this distance was calculated using the simulation described in appendix.

3.2. Doppler-broadened 1s–2p linewidth

In addition to measuring the velocity component normal to the target surface, the experimental arrangement was also used to find the spread in Ps velocities along the direction of propagation of the lasers. The wavelength of the UV laser was tuned across the 1s–2p transition and lifetime spectra recorded. Photoionization was quantified by the parameter S [17], which is the difference in the delayed fraction f, compared to background measurements with the laser far from resonance f_b:

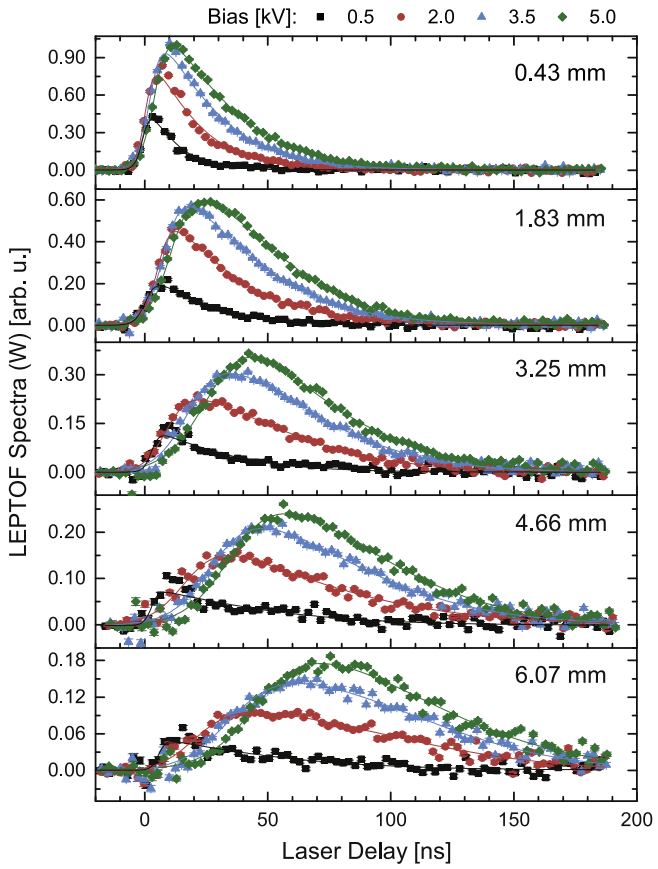

Figure 7. The mean, background-subtracted and o-Ps decay corrected ionization signal measured in a 4 ns interval coincident with applied UV and green lasers, averaged over ~120 measurements per data point. The lasers were positioned at various distances from the target, which was biased from 500 V to 5 kV. The solid lines are asymmetric double sigmoid fits to the points (see text).

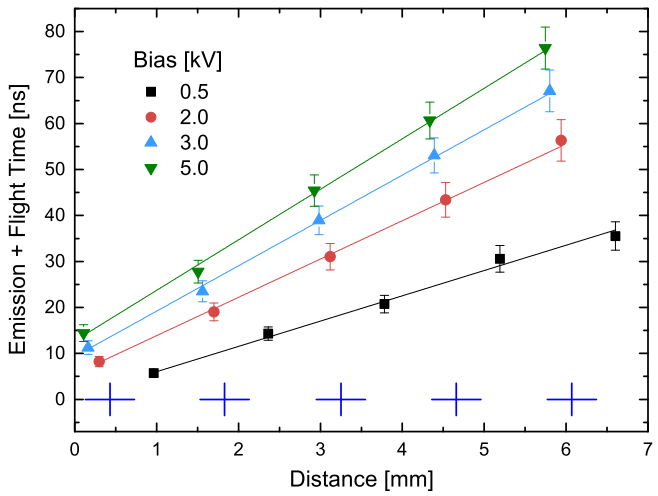

Figure 8. The mean time interval between positron implantation and Ps arrival at each measurement position. The solid lines show linear fits to each data set. The vertical error-bars represent an estimate of the standard error of the mean (SEM). The blue crosses mark the various positions of the laser beam and illustrate the FWHM of its profile (0.6 mm) and the time-width (6 ns) of the pulse.

$$S = \frac{f_b - f}{f_b}. \tag{2}$$

Figure 9 shows S plotted against the wavelength of the UV laser. A Gaussian function of the form $A \exp\left[-(\lambda - \lambda_0)^2/(2\sigma^2)\right]$ has been fitted to the data points, from which the rms speed in the direction parallel to the laser was estimated by assuming the profile is dominated by non-relativistic Doppler broadening

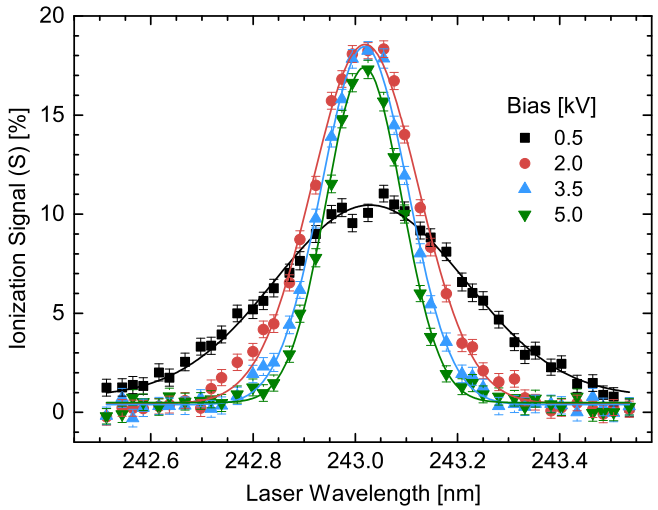

Figure 9. The Doppler-broadened linewidth of the 1s–2p transition of Ps, as measured by REMPI via $n = 2$. The solid lines are Gaussian fits to the points. Note, for these measurements no slit was used to reduce the UV beam profile.

$$v_x^{\mathrm{rms}} = \frac{c\sigma}{\lambda_0}. \tag{3}$$

We observe that for positrons implanted into the silica at higher energies, the Doppler profile of the resultant Ps distribution is narrowed, indicating Ps cooling within the porous structure [21]. This is also evident in figure 8, where increasing beam energies are found to result in slower centre-of-mass motion of the Ps distribution along z.

These data highlight the fact that LEPTOF measurements are naturally velocity selective along the direction of the probe lasers: the limited spectral overlap of the ~100 GHz wide excitation laser with the Doppler-broadened 1s–2p transition will select a subset of the slowest Ps atoms. This explains why the largest LEPTOF signal (W) was obtained for the highest target bias (i.e., coldest Ps), even though the yield is reduced—see figures 2 and 7. In principle LEPTOF measurements could be performed by scanning the laser wavelength and using the signal integrated over the entire Doppler profile, although this would significantly increase the data acquisition time. Alternatively, one could use a laser with sufficient bandwidth to cover the entire profile, or a Doppler-free two-photon excitation scheme [38] could be employed to probe the atoms (albeit with lower efficiency).

3.3. Positronium cooling and emission

The gradients of the linear fits in figure 8 were used to estimate the mean perpendicular velocity component of Ps as a function of target bias voltage. This is plotted in figure 10(a), which indicates that the Ps kinetic energy E_z, associated with the centre-of-mass motion in the direction perpendicular to the target surface, tends toward a lower limit of ~40 meV, in agreement with TOF measurements made by Crivelli *et al* using nominally identical samples [22]. A similar trend is evident in the rms velocity deduced from the widths of the Doppler profiles. The apparent agreement between the corrected LEPTOF (v_z) and the Doppler (v_x^{rms}) measurements is not necessarily significant; we emphasize the former is a measure of the mean velocity away from the target, whereas the latter is an indication of the velocity spread along the direction of propagation of the UV laser.

In conventional Ps TOF spectroscopy a correction factor proportional to t^{-1} is usually applied to the data to account for the fact that the probability of detecting a Ps atom depends on how long it spends in the field of view of the detector e.g., [13, 37, 39]. The LEPTOF equivalent of this correction is similar but must also take into account the probability that an atom is ionized by the laser field. This depends on the spatial profile and intensity of both the excitation and ionization lasers, as well as the Ps speed, as described in appendix. The corrections discussed in section 3.1 are only approximate as the simulations do not fully take into account the (unknown) Ps distributions. To illustrate the significance of accounting for these effects, we plot estimates of the velocity and emission times found without use of the correction functions (figure 10(a), grey points).

The lowest Ps energies observed are always above what might be expected were Ps to thermalize completely with the room temperature bulk (25 meV). This is due to the Ps confinement energy [21–23] in the nano-pores, which is approximately 30 meV for the ~ 5 nm diameter pores [22]. These data demonstrate that for positron beam energies above 2 keV the resulting Ps is approaching the quantum confinement regime.

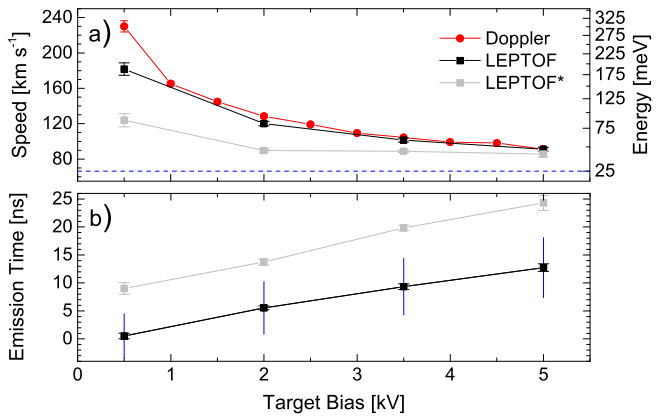

Figure 10. (a) The rms speed of the Ps atoms in the direction parallel (v_x^{rms}) to the probe laser as measured by 1s–2p Doppler spectroscopy, and the velocity component though the laser (v_z) found by LEPTOF spectroscopy. The horizontal dashed line indicates 25 meV Ps (300 K). (b) The mean emission time from the sample as determined by extrapolating the fits of figure 8 to zero distance. The light grey data-points (*) indicate values estimated from uncorrected LEPTOF spectra. The error-bars represent the uncertainty in fitting the arrival time (figure 8); they do not include the uncertainty in the applied correction function. The blue vertical bars in (b) illustrate a conservative estimate of the scope for systematic error in the measured emission time, as the linear sum of the standard deviation of the laser pulse ($\sigma_t = 2.55$ ns) and the error found assuming the laser position is offset by one standard deviation of its width ($\sigma_x = 0.255$ mm) divided by the measured velocity.

We estimate the mean Ps emission time from the sample by extrapolating the linear fits plotted in figure 8 to zero distance (see figure 10(b)). Emission times of the order of 10 ns are found at the highest implantation energy, even with the applied correction. This is in accordance with previous measurements made using similar targets (but with smaller pores) [26]. In that work the energy dependence of the Ps decay rate was used to infer the rate of emission into vacuum, and the analysis includes assumptions regarding Ps diffusion, which we now know to be incorrect for quantum confined Ps [24]; here we measure the time taken for Ps to leave the sample and then travel a known distance. However, we reiterate that the uncertainty in this measurement does not account for the uncertainty in modelling the interaction between the atoms and laser. Whilst the velocity would not be affected by a systematic shift in the location within the beam of the mean interaction point, the emission times would be. To illustrate this we calculate the sum of the standard deviation of the laser pulse ($\sigma_t = 2.55$ ns) and the error found assuming the laser position is offset by one standard deviation of its width ($\sigma_x = 0.255$ mm) divided by the measured velocity. This is represented by the blue vertical bars in figure 10(b).

4. Conclusions

The LEPTOF technique has facilitated a direct measurement of Ps emission times from porous silica (figure 10). The measurements provide clear evidence for delayed Ps emission over the range of $(0.5 \pm 0.5 \pm 4.0)$ ns to $(12.7 \pm 0.7 \pm 5.4)$ ns, which is consistent with previous lifetime-based measurements using similar target materials [26]. We find that Ps thermalization into the quantum confined regime is largely complete within ~5 ns.

Since the mean stopping depth of a positron pulse depends on the implantation energy as K^{η} [4, 40, 41] (where η is a material specific constant, estimated to be ~1.6 for silica), we would expect the emission time for thermalized Ps to be roughly proportional to $K^{3.2}$ [21], whereas a near linear relationship of roughly 3 ns per keV was observed. This expectation is based on Ps reaching the surface via a random-walk diffusion process. The observed dependence may instead be the result of anomalous tunnelling and diffusion processes in the porous structure, as have been identified previously via unexpectedly high Ps–Ps scattering rates [24]. While restricting Ps atoms to a smaller set of pores would be expected to increase Ps–Ps scattering, it would not necessarily make it easier for Ps atoms to escape into vacuum; this would occur only if the interconnectivity of the pores were particularly favourable for such. Our data suggest that this is perhaps the case.

LEPTOF spectroscopy is advantageous in some areas, but it is limited in others. The relatively narrow bandwidth of our UV laser preferentially selects atoms with a low velocity component in the direction of propagation of the UV radiation (v_x). This must be taken into account before any conclusions can be drawn regarding the entire Ps ensemble in any given measurement. The threshold Ps speed through the laser, above which photoionization becomes unlikely, was low enough to have slightly distorted the TOF spectra towards later times. A simple correction applied to the spectra produced reasonable results, however, a more rigorous simulation of the Ps atoms' interaction with the two lasers might improve on this. Accordingly, the uncorrected

data of figure 10 represent an upper limit on the emission times (and lower limit on the measured velocity), since the over-counting of slow Ps will have skewed the distribution to later times.

The velocity dependence of Ps ionization also sets a practical limit to the energy of Ps atoms that can be studied using this method. Ps atoms with energies much greater than 1 eV would not be efficiently ionized and/or would require greater laser powers than have been used here. Conventional TOF spectroscopy is better suited to such Ps energies (e.g., [15, 39, 42]), but LEPTOF spectroscopy is more useful for studies of low energy Ps. For example, Ps cooled to 10 K would have a speed of approximately 10^6 cm s^{-1} and would travel about 1 mm in its ground-state lifetime. It is a relatively simple matter to focus a laser to a few tens of microns, and indeed doing so would eliminate many of the systematic uncertainties associated with determining the Ps ionization position (see appendix). Thus, very cold Ps can easily be studied using LEPTOF methods. Using colder Ps would also make it easier to excite all atoms, either by improving the overlap between the laser and the Doppler-broadened bandwidth, or by making it possible to focus the laser to a smaller spot and perform Doppler-free two-photon excitation.

Understanding the cooling and diffusion processes of Ps confined in porous materials is of vital importance for many different types of experiment. One such area of study involves high-density Ps, wherein a long-standing goal is the production of a positronium Bose–Einstein condensate (BEC) [43]: the much anticipated precursor to the gamma-ray laser [44]. For presently feasible Ps densities this is expected to occur at temperatures in the range of 10–100 K. Since Ps is known to cool from over 10 000 K to close to 300 K in porous silica films with minimal losses, only a relatively small advancement (e.g. engineered pore morphologies [45]) might be required to make the Ps BEC an experimental reality [46].

If quantum confinement effects can be mitigated, modified mesoporous materials could prove to be a valuable source of cold Ps. This may be achieved using structures with larger pore sizes, although such materials tend to be less efficient Ps converters and are less stable mechanically. Alternative geometries may offer colder Ps [37], and cooling rates could be increased by the use of surface-adsorbate based Ps cooling mechanisms [47]. Materials that emit Ps atoms into vacuum at low velocities are desirable for experiments involving Ps interactions with tightly focused laser fields [48], and also to reduce transit-time broadening and second-order Doppler effects in precision spectroscopy measurements [49]. Indeed almost any experiment involving Ps-laser interactions will benefit from a source of colder Ps, owing to the reduction in Doppler broadening of single-photon transitions (e.g., [21]).

To summarize, LEPTOF spectroscopy was used to measure the kinetic energy of Ps emitted from a mesoporous silica film. We observed that Ps atoms were emitted at lower speeds when the incident positron beam energy was increased, and found that the Ps energy approached a non-thermal confinement limit, as has been observed in previous TOF [22] and Doppler measurements [21] made using similar Ps converters. By extrapolating our TOF data to zero distance we estimated the time taken for Ps to escape from the sample into vacuum. We found a mean emission time of around 10 ns for an incident positron beam energy of 5 keV, which is consistent with a tunnelling-limited diffusion process characteristic of quantum confinement [26]. However, the observed dependence of the emission time upon the positron implantation energy indicates that Ps diffusion occurs through a subset of the available pore volume, in accordance with previous observations [24].

Acknowledgments

The authors are grateful to R Jawad and J Dumper for technical assistance, and to L Liszkay for providing silica targets. This work was funded in part by the Department of Physics and Astronomy, and the Faculty of Mathematical and Physical Sciences at University College London, the Leverhulme trust (grant number RPG-2013-055) and the EPSRC (grant number EP/K028774/1).

Appendix. Positronium-laser interactions

The interaction of Ps atoms with laser radiation was modelled numerically by considering Rabi oscillations between the 1s and 2p states driven by UV light, and the subsequent photoionization of 2p atoms by a 532 nm laser. Only atoms on resonance with the UV laser were considered (i.e. Doppler shifts were neglected).

The Cartesian coordinate system used here is defined such that the surface of the Ps converter lies parallel to the plane of xy. The UV laser traverses the interaction region horizontally, parallel to the x-axis, and the vertical direction is given by $\hat{y}$. The z-axis is aligned to the long-axis of the positron beamline and represents the direction along which the TOF of positronium was measured; the origin is defined as the point where this intersects the laser path.

The $\lambda = 243$ nm laser beam was measured to have a Gaussian intensity profile along the z-axis ($\sigma_z = 268$ μm), with a 6 mm full-width 'top-hat' distribution in the vertical (y) direction. The LEPTOF experiments were

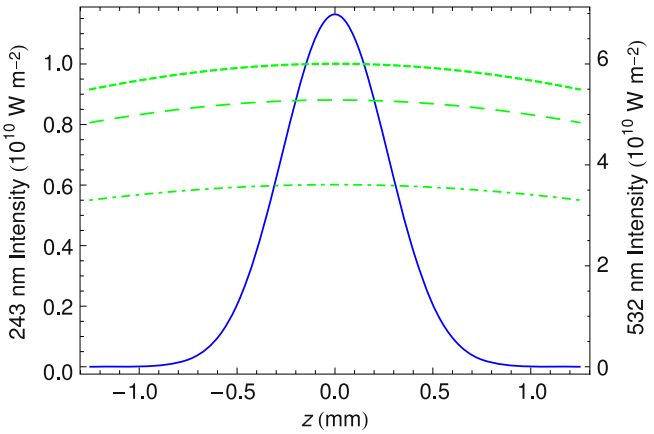

Figure A1. Peak intensity profiles along z of the UV beam (blue), and the 532 nm beam at $y = 0$ mm (green, dotted), $y = 1.5$ mm (green, dashed), and $y = 3$ mm (green, dashed–dotted). The curves are Gaussian fits to beam profiles measured using a travelling knife-edge.

performed with UV beam energies of 300 μJ per pulse. The two transverse intensity profiles of the visible, $\lambda = 532$ nm beam were Gaussian, with equal widths $\sigma_y = \sigma_z = 3.0$ mm. Photoionization from the 2p state was modelled with peak visible intensities in the range of 2×10^{10} to 18×10^{10} W m^{-2}. The laser beams were both collimated and approximately collinear within the region where they intersected the Ps atoms. Figure A1 shows the profile of the UV beam (blue line) as a function of z, at the moment of peak intensity. Also shown is the intensity profile of the 20 mJ, $\lambda = 532$ nm beam along z, for the vertical positions of $y = 0$ mm (green, dotted), $y = 1.5$ mm (green, dashed), and $y = 3.0$ mm (green, dotted–dashed).

To analyze the interaction process we calculated the probability of photoionization of Ps atoms with transit speeds in the range from 12.5 to 500 km s^{-1}. For each speed the photoionization probability was calculated for an ensemble of atoms covering a range of initial positions: from $z_{\rm init} = -2$ to -0.5 mm in steps of 0.5 mm, and $y_{\rm init} = -3$ to 3 mm in steps of 0.1 mm, with each atomic trajectory starting at a time 7.6 ns prior to the lasers reaching peak intensity. In this way the distribution of the atomic ensemble along y covered the full height of the UV beam profile, which is important as the 532 nm intensity changes non-negligibly over this range (see figure A1), and the distribution in the z-direction allows the photionization probability to be calculated over a range of laser delays. The lasers do not vary significantly along their path, therefore only the plane of $x = 0$ was considered.

As the Ps atoms travel along the z-direction they first encounter the 532 nm laser beam, however they do not significantly interact with it. Once they reach the UV beam the 243 nm radiation drives Rabi oscillations between the 1s and 2p states. To simplify the calculations the UV beam was assumed to be transform-limited. Figure A2 shows the Rabi oscillations driven in atoms with three different speeds: 50, 100 and 150 km s^{-1}. As the atoms begin to traverse the UV beam the Rabi frequency starts to increase. After moving only 200 μm into the beam it exceeds 6 GHz and atoms travelling at 50 km s^{-1} will have experienced ten 1s–2p oscillations. Faster atoms penetrate further into the laser field before experiencing a similar number.

We assume that once an atom has made its first Rabi oscillation it then spends half its time in the 2p state. Using the spatial variation in UV intensity during the pulse, we then determined for each atom the region and times over which this occurs. The cross-section for photoionization from the 2p state with 532 nm radiation is $\sigma_{\rm PI} \simeq 3 \times 10^{-21}$ m^2 [50]. This was then combined with the intensity profile of the visible radiation and the regions where Ps atoms are excited by the UV laser, to find the photoionization probability integrated along each atom's flight path. For each speed and initial z-position the mean photoionization probability was calculated over the range of y-positions. The mean probabilities for each initial z-position were then combined to give the overall photionization probability for a given speed. This effectively gives the overall efficiency of our photoionzation scheme averaged over a reasonable range of laser delays. Figure A3 shows the photoionization probability as a function of speed calculated with peak 532 nm intensity in the range from 2×10^{10} to 18×10^{10} W m^{-2}. For the case of a peak intensity of 6×10^{10} W m^{-2}, which corresponds to the 20 mJ used in the experiments presented here, we can photoionize all the atoms for which $v_z \lesssim 250$ km s^{-1}, above which the photoionization probability decreases. For these greater speeds the atoms pass so quickly through the laser beams that their reduced interaction time limits the photionization probability.

The photoionization probabilities calculated with greater visible intensities show similar behaviour, except the threshold at which the photoionization probability begins to fall is increased to greater speeds. With a peak

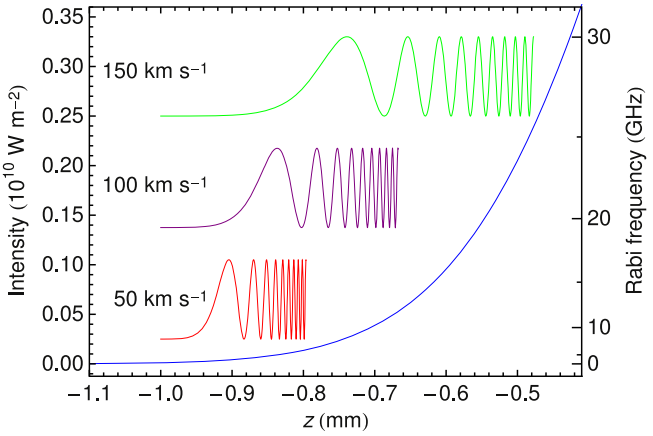

Figure A2. Rabi oscillations between the 1s and 2p states of Ps atoms travelling at 50 km s^{-1} (red), 100 km s^{-1} (purple), and 150 km s^{-1} (green) driven by the 243 nm radiation of the UV beam (blue). For each atom the Rabi oscillations are displayed up to the position at which 10 oscillations to the 2p state have been made.

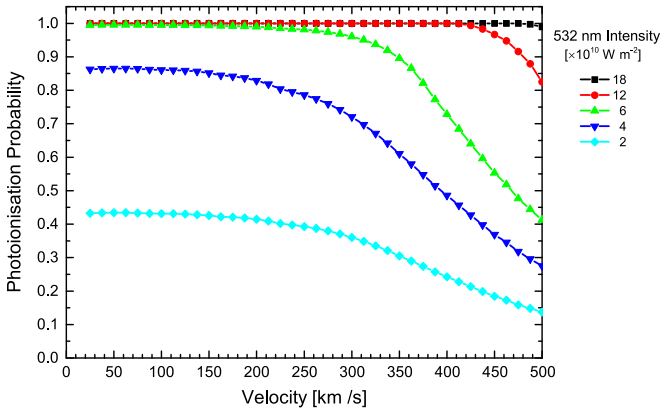

Figure A3. Calculated photoionization probability for Ps atoms travelling through the laser beams, for a range of visible (532 nm) laser intensities. A peak intensity of 6×10^{10} W m^{-2} (green triangles) is equivalent to the 20 mJ per pulse used in the experiments. For each point the simulated atomic ensemble covers a range of positions in the y-direction from −3 to 3 mm (i.e. the full height of the UV laser beam).

532 nm intensity of 18×10^{10} W m^{-2} atoms covering almost the whole range of speeds studied are photoionized. Conversely, for peak intensities less than 6×10^{10} W m^{-2} this threshold is reached at lower speeds and the maximum probability also drops below one, as the average exposure time required for photoionization in the weaker fields approaches the pulse duration. It has been found that the faster atoms are photoionized more efficiently when they start further from the laser beam. In this way they are travelling into the beams as the laser intensity increases, thus maximizing their interaction with high-intensity radiation. The slower atoms, however, experience greater photoionization probability when they start close to (or inside) the lasers, and do not travel far during the pulse.

Figure A3 suggests that the overlapping UV and visible laser beams create a well-defined volume for REMPI of ground-state Ps atoms, which allows us to set limits on the velocities of Ps which can contribute to LEPTOF spectra. For the laser parameters used in this work, atoms entering the interaction region at speeds below 300 km s^{-1} are expected to be photoionized with near unity probability.

The calculation is simplistic and does not attempt to include the exact temporal and spatial distribution of the atoms, thus the results are not directly comparable with the experimental data. For example, the spatial distribution has been treated as uniform over the vertical extent of the UV beam, whereas it is likely to be weighted towards the centre of the beam ($y = 0$). However, the purpose of this simple analysis is to provide a basic model of the interaction with laser radiation, without making assumptions regarding the atomic ensemble, verifying that by using the LEPTOF technique it is possible to detect a large portion of the incident Ps atoms, over a broad range of speeds.

More comprehensive simulations would be useful and could in principle be used to generate a function to fully correct LEPTOF spectra, removing any bias towards observing slower atoms or over-counting effects due to the finite size of the interaction region. However these would require complete velocity distributions of the Ps atoms emitted from the target. A complete simulation of the Ps-laser interaction should also include the small contribution to the 'ionization' signal of magnetically quenched (but not ionized) $n = 2$ positronium [51, 52], which is not entirely negligible in the ~100 G field of the target region [53].

References

[1] Rich A 1981 *Rev. Mod. Phys.* **53** 127
[2] Charlton M and Humberston J W 2001 *Positron Physics* (*Cambridge Monographs on Atomic, Molecular and Chemical Physics* vol 2) 1st edn (Cambridge: Cambridge University Press)
[3] Krause-Rehberg H L R 1999 *Positron Annihilation in Semiconductors* (*Solid-State Sciences* vol 127) (Berlin: Springer)
[4] Schultz P J and Lynn K G 1988 *Rev. Mod. Phys.* **60** 701
[5] Paulin R and Ambrosino G 1968 *J. Phys. France* **29** 263
[6] Canter K F, Mills A P Jr and Berko S 1974 *Phys. Rev. Lett.* **33** 7
[7] Mills A P Jr and Crane W S 1984 *Phys. Rev. Lett.* **53** 2165
[8] Mills A P Jr and Crane W S 1985 *Phys. Rev.* A **31** 593
[9] Sferlazzo P, Berko S, Lynn K G, Mills A P Jr, Roellig L O, Viescas A J and West R N 1988 *Phys. Rev. Lett.* **60** 538
[10] Gidley D W, Peng H G and Vallery R S 2006 *Annu. Rev. Mater. Res.* **36** 49
[11] Cassidy D B, Hisakado T H, Tom H W K and Mills A P Jr 2011 *Phys. Rev. Lett.* **106** 133401
[12] Mills A P Jr, Pfeiffer L and Platzman P M 1983 *Phys. Rev. Lett.* **51** 1085
[13] Howell R H, Rosenberg I J, Fluss M J, Goldberg R E and Laughlin R B 1987 *Phys. Rev.* B **35** 5303
[14] Gidley D W, Frieze W E, Dull T L, Yee A F, Ryan E T and Ho H M 1999 *Phys. Rev.* B **60** R5157
[15] Yu R S, Ohdaira T, Suzuki R, Ito K, Hirata K, Sato K, Kobayashi Y and Xu J 2003 *Appl. Phys. Lett.* **83** 4966
[16] Vallery R S, Zitzewitz P W and Gidley D W 2003 *Phys. Rev. Lett.* **90** 203402
[17] Cassidy D B, Bromley M W J, Cota L C, Hisakado T H, Tom H W K and Mills A P Jr 2011 *Phys. Rev. Lett.* **106** 023401
[18] Cassidy D B, Deng S H M, Greaves R G, Maruo T, Nishiyama N, Snyder J B, Tanaka H K M and Mills A P Jr 2005 *Phys. Rev. Lett.* **95** 195006
[19] Cassidy D B, Hisakado T H, Tom H W K and Mills A P Jr 2012 *Phys. Rev. Lett.* **108** 133402
[20] Liszkay L *et al* 2012 *New J. Phys.* **14** 065009
[21] Cassidy D B, Crivelli P, Hisakado T H, Liszkay L, Meligne V E, Perez P, Tom H W K and Mills A P Jr 2010 *Phys. Rev.* A **81** 012715
[22] Crivelli P, Gendotti U, Rubbia A, Liszkay L, Perez P and Corbel C 2010 *Phys. Rev.* A **81** 052703
[23] Mariazzi S, Salemi A and Brusa R S 2008 *Phys. Rev.* B **78** 085428
[24] Cassidy D B and Mills A P Jr 2011 *Phys. Rev. Lett.* **107** 213401
[25] Fischer C G, Weber M H, Wang C L, McNeil S P and Lynn K G 2005 *Phys. Rev.* B **71** 180102
[26] Cassidy D B, Hisakado T H, Meligne V E, Tom H W K and Mills A P Jr 2010 *Phys. Rev.* A **82** 052511
[27] Surko C M and Greaves R G 2004 *Phys. Plasmas* **11** 2333
[28] Mills A P Jr and Pfeiffer L 1979 *Phys. Rev. Lett.* **43** 1961
[29] Cassidy D B, Deng S H M, Greaves R G and Mills A P Jr 2006 *Rev. Sci. Instrum.* **77** 073106
[30] Mills A Jr 1980 *Appl. Phys.* **22** 273
[31] Liszkay L *et al* 2008 *Appl. Surf. Sci.* **255** 187
[32] Liszkay L *et al* 2008 *Appl. Phys. Lett.* **92** 063114
[33] Cassidy D B and Mills A P Jr 2007 *Nucl. Instrum. Methods* A **580** 1338
[34] Cassidy D B, Deng S H M, Tanaka H K M and Mills A P Jr 2006 *Appl. Phys. Lett.* **88** 194105
[35] Demtröder W 2003 *Laser Spectroscopy* 3rd edn (New York: Springer)
[36] Cassidy D B, Hisakado T H, Tom H W K and Mills A P Jr 2011 *Phys. Rev. Lett.* **106** 173401
[37] Mariazzi S, Bettotti P and Brusa R S 2010 *Phys. Rev. Lett.* **104** 243401
[38] Hänsch T W, Lee S A, Wallenstein R and Wieman C 1975 *Phys. Rev. Lett.* **34** 307
[39] Sferlazzo P, Berko S and Canter K F 1987 *Phys. Rev.* B **35** 5315
[40] Mills A P Jr and Wilson R J 1982 *Phys. Rev.* A **26** 490
[41] Algers J, Sperr P, Egger W, Kögel G and Maurer F H J 2003 *Phys. Rev.* B **67** 125404
[42] Nagashima Y, Morinaka Y, Kurihara T, Nagai Y, Hyodo T, Shidara T and Nakahara K 1998 *Phys. Rev.* B **58** 12676
[43] Platzman P M and Mills A P Jr 1994 *Phys. Rev.* B **49** 454
[44] Wang Y H, Anderson B M and Clark C W 2014 *Phys. Rev.* A **89** 043624
[45] He C, Wang S, Kobayashi Y, Ohdaira T and Suzuki R 2012 *Phys. Rev.* B **86** 075415
[46] Morandi O, Hervieux P A and Manfredi G 2014 *Phys. Rev.* A **89** 033609
[47] He C, Ohdaira T, Oshima N, Muramatsu M, Kinomura A, Suzuki R, Oka T and Kobayashi Y 2007 *Phys. Rev.* B **75** 195404
[48] Balling P, Fregenal D, Ichioka T, Knudsen H, Kristiansen H P E, Merrison J and Uggerhøj U I 2004 *Nucl. Instrum. Methods* B **221** 200
[49] Fee M S, Mills A P Jr, Chu S, Shaw E D, Danzmann K, Chichester R J and Zuckerman D M 1993 *Phys. Rev. Lett.* **70** 1397
[50] Bethe H and Salpeter E 1957 *Quantum Mechanics of One and Two Electron Atoms* (Berlin: Springer)
[51] Curry S M 1973 *Phys. Rev.* A **7** 447
[52] Dermer C D and Weisheit J C 1989 *Phys. Rev.* A **40** 5526
[53] Ziock K P, Dermer C D, Howell R H, Magnotta F and Jones K M 1990 *J. Phys. B: At. Mol. Opt. Phys.* **23** 329